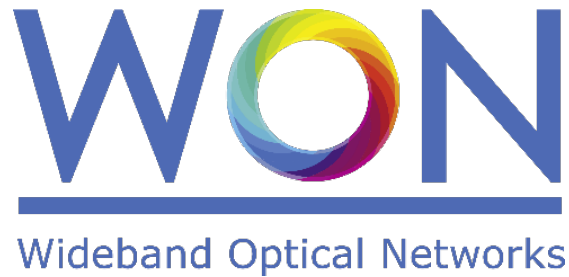


Marie Skłodowska-Curie (MSCA) – Innovative Training Networks (ITN)  
H2020-MSCA-ITN European Training Networks



## Wideband Optical Networks [WON]

Grant agreement ID: 814276

### **WP4 – Transceiver components design**

### **Deliverable D4.1 Transceiver Concept and Target Specifications**



*This project has received funding from the European Union's Horizon 2020 research and innovation programme under the Marie Skłodowska-Curie grant agreement 814276.*

## Document Details

Work Package	WP4 – Transceiver components design
Deliverable number	D4.1
Deliverable Title	Transceiver Concept and Target Specifications
Lead Beneficiary:	Fraunhofer HHI
Deliverable due date:	31 October 2019
Actual delivery date:	8 June 2020
Dissemination level:	Public

## Project Details

Project Acronym	WON
Project Title	Wideband Optical Networks
Call Identifier	H2020-MSCA-2018 Innovative Training Networks
Coordinated by	Aston University, UK
Start of the Project	1 January 2019
Project Duration	48 months
Project Website:	<a href="https://won.astonphotonics.uk/">https://won.astonphotonics.uk/</a>
CORDIS Link	<a href="https://cordis.europa.eu/project/rcn/218205/en">https://cordis.europa.eu/project/rcn/218205/en</a>

## WON Consortium

Consortium member	Legal Entity Short Name
Infinera Germany	INF G
Aston University	Aston
Danmarks Tekniske Universitet	DTU
VPIphotonics GmbH	VPI
Infinera Portugal	INF PT
Fraunhofer HHI	HHI
Politecnico di Torino	POLITO
Technische Universiteit Eindhoven	TUE
Universiteit Gent	UG
Keysight Technologies	Keysight
Finisar Germany GmbH	Finisar
Orange SA	Orange
Technische Universitaet Berlin	TUB
Instituto Superior Tecnico, University of Lisboa	IST

## Abbreviations and Acronyms:

EC	European Commission
ETN	European Training Network
MZI	Mach-Zehnder interferometer
DCI	Data Center Interconnect

DSP	Digital Signal Processor
DAC	Digital-to-Analogue Converter
DRV	Driver Amplifier
LS	Laser Source
InP	Indium Phosphide
MMI	Multimode Interferometer
PIC	Photonic Integrated Circuit

## Contents

EXECUTIVE SUMMARY .....	5
1. OVERVIEW TRANSCEIVER CONCEPT AND COMPONENTS.....	5
2. LASER.....	7
2.1 Concept.....	7
1.2 Target Specifications of the wideband tuneable laser source.....	8
3. DUAL-POLARIZATION I/Q MODULATOR.....	8
3.1 Concept.....	8
3.2 Target Specifications of the wideband dual-polariztaion I/Q modulator .....	10
4. INTRADYNE COHERENT RECEIVER FRONTEND .....	13
5. DIGITAL SIGNAL PROCESSING .....	14
5.1 Transmitter-Side DSP .....	14
5.2 Receiver-Side DSP .....	14
REFERENCES .....	16

## EXECUTIVE SUMMARY

The present scientific deliverable is a part of the Work Package 4 “Transceiver components design” of the ETN project WON “Wideband Optical Network”, funded under the Horizon 2020 Marie Skłodowska-Curie scheme Grant Agreement 814276.

This first deliverable D4.1 “Transceiver Concept and Target Specifications” of WP4 “Transceiver components design” describes the main concepts for a multi-band optical transceiver, incorporating its key components such as (1) a multi-band tuneable laser source, (2) a multi-band dual-polarization I/Q modulator, (3) a multi-band coherent receiver and (4) a digital signal processor. For each component, the state-of-the-art is reviewed and critical issues for multi-band design are described. Based on first architectural and technological considerations and simulations, target specifications for the individual components are derived. For the two main components developed in WON, the multi-band laser source and the dual-polarization I/Q modulator, the target specifications are as follows.

*Table 1: Target specifications of the multiband tuneable laser source.*

Parameter	Target Specification
Tuning range	> 200 nm; quasi-continuous tuning
Output power	> 10 dBm
Side mode suppression ratio (SMSR)	> 40 dB
Linewidth	< 100 kHz
RIN (relative intensity noise)	< -130 dB/Hz

*Table 2: Target specifications of the dual-polarization I/Q modulator*

Parameter	Target Specification
Insertion Loss	< 15 dB
Half wave Voltage ( $V_{\pi}$ )	< 3 V
Extinction Ratio	> 15 dB

## 1. OVERVIEW TRANSCEIVER CONCEPT AND COMPONENTS

As demand for communication data-traffic rises at an accelerating pace, with about a million minutes of video content crossing the IP network every second [1], the pursuit for enhanced designs of optical components drives research throughout the Photonics field. In this context, a key component in communication systems is the optical transceiver, which plays a vital role in the task of delivering high-speed transmission at elevated performance requirements. The basic concept of this device consists in the ability of transmitting and receiving data for a broad range of applications (e.g., long-haul/undersea, metro-telecom, data center interconnect (DCI), intra-DCI). Besides the multiple purposes of application, the use of transceivers is also very compelling because it is a cost-effective solution based on photonic integration, which permits a high flexibility in communication networks and therefore is a major building block towards the scalability of the telecommunication infrastructure in the next years.

Since 2016, 100G optical transceivers (state-of-the-art) dominate the market [2], kicked-off by the pressing requirements of Internet content providers and the growth of their DCs. Next generation transceivers aim at supporting data-rates up to 400 Gb/s, 800 Gb/s and 1.0 Tb/s [3],[4], which follows a 10 times increase from existing systems. Besides the recent advances of sophisticated technologies to promote even higher data rates, research also focusses on the usage of multiple optical bands

[5],[6] as means to provide higher bandwidth and unburden the current technology limitations. Studies focussed on multiband transceiver design have already been initialized [7] and motivate discussions as the one derived in this text.

As mentioned before, a transceiver is a device that can perform tasks of a transmitter (TX) and a receiver (RX). In most cases, a transceiver contains a transmitter and a receiver sharing the same physical infrastructure (housing and circuitry). Figure depicts an exemplary block diagram of a transceiver for digital coherent systems. These systems have gained increasing commercial interest because of its promising potential for promoting high capacity transmission, which consequently leads to a reduced cost per transmitted bit. Briefly, the transmitter design of coherent transceivers is composed by the serial operation of six main blocks: DSP (Digital Signal Processor), DAC (Digital-to-Analogue Converter), DRV (Driver Amplifier), LS (Laser Source), Optical IQ Modulator and Polarization Combiner. In summary, the electrical signal, before being transmitted, is pre-processed (encoding and filtering) at the DSP and these binary data are afterwards converted via the use of DAC. As a result, the signal is delivered to the DRV so that it can be amplified to an RF level and properly drive the optical modulator. The modulator, subsequently, handles the electrical-optical conversion (cf. section 2.3 for a dedicated discussion on the modulator design). In order to generate a light beam, a LS is used at the transmitter block. At the very end of the transmitter side, lies the polarization combiner, responsible for polarization-division multiplexing (PDM) to double the capacity of transmitted information. The receiving part follows a similar topology, except that the signal now undergoes an OE (optical-electrical) conversion. The first component encountered by the optical signal is the Polarization Beam Splitter, which separates the incoming light into two independent single-polarization beams. These beams are then forwarded to the Optical 90-degree hybrids where the in-phase and quadrature components (per polarization) are finally separated and the electrical-optical conversion can finally be performed by the photodiodes. After that, the digital representation of the signal is obtained via the use of ADCs (Analogue-to-Digital Converter) which provide binary data to the DSP block for decoding and filtering purposes. It is good to bear in mind that the described architecture narrates the basic block diagram of a transceiver for digital coherent systems, which is the one examined in this work. Despite eventual variations in terms of design are possible, the core concept of an optical transceiver resides in the functioning of a transmitter/receiver (E-O/O-E conversion), usually mounted on a single chip which permits gains in terms of costs, flexibility and scalability.

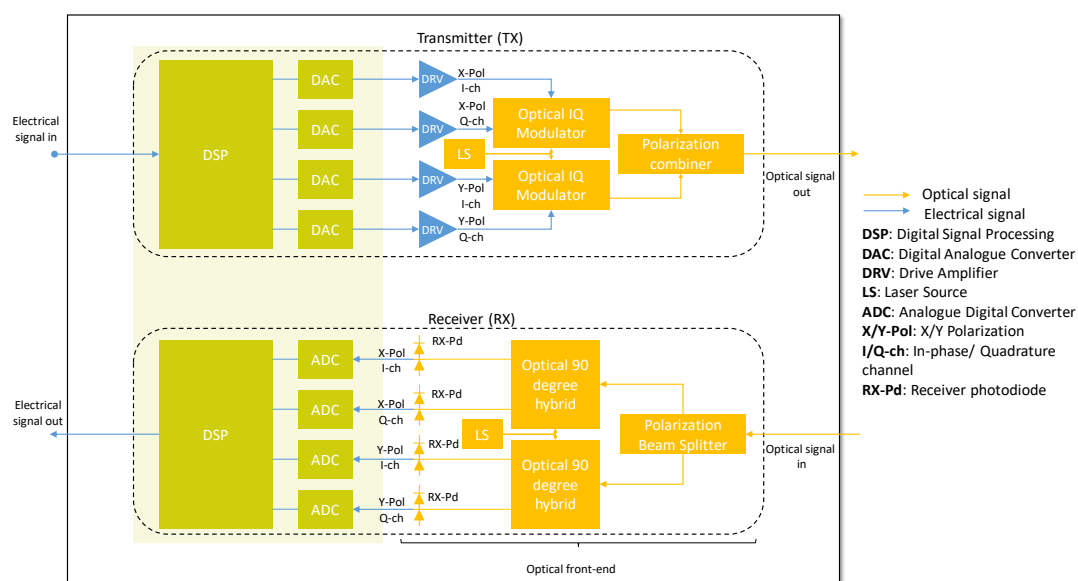


Figure 1: Diagram of a conventional digital coherent system transceiver.

Nowadays, the vast majority of transceivers are designed to operate in the C band (1530 nm - 1565 nm) not only because it overlaps with the low-attenuation regime of most of the currently deployed optical fibres, but also because transceiver component properties behave very stable within this spectral domain, for materials such as InP and LiNbO<sub>3</sub> (commonly used in transceiver fabrication).

The project WON targets true multiband transceivers, which are capable to operate over the full multiband regime (O to L band, 1260 nm – 1625 nm). In this respect, the project will identify the main challenges in scaling the transceiver subcomponents to such a wideband operational window. For instance, integrated beam splitters (preferably implemented with MMI – multimode interferometer), are fundamental building-blocks in the design of optical IQ modulators, however, it is known [8] that their operability in the multiband regime (O to L band, 1260 nm – 1625 nm) imposes significant variations in terms of insertion loss, power imbalance and phase error. This work will also present (section 2.3.2) that when incorporating these couplers into the design of InP-based MZI (Mach-Zehnder Interferometer), which are present inside optical IQ modulators, slight variations in power imbalance can lead to major disruption in coherent optical systems and disable the feasibility of transmission in broad portions of the spectrum. Thus, in order to promote the advance towards these new spectral frontiers, a primary investigation on fundamental transceiver components is required to predict performance analysis and build target specifications that will allow the understanding of interventions to enable the future deployment of these devices.

The following sections deal with the main transceiver subcomponents: the low-linewidth widely tuneable laser source (section 0), the wideband dual-polarization I/Q modulator (section 0), the intradyne coherent receiver (section 0), and finally the digital signal processor (section 0).

## 2. LASER

### 2.1 Concept

The wideband transceiver requires a wideband tuneable laser source. The wavelength coverage of a semiconductor laser is determined by the bandwidth of the gain medium and the losses in the laser cavity. Typically, the tuning range of a single semiconductor laser is limited to 50 nm - 100nm. In order to cover a broader wavelength range, multiple III-V gain elements need to be co-integrated to form an ultra-widely tuneable laser, as shown in Figure 1.

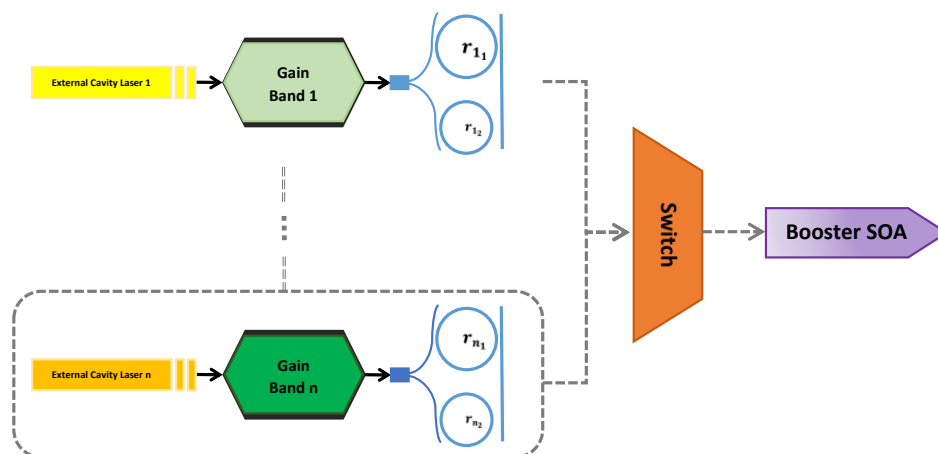


Figure 1: Layout of the wideband tuneable laser structure: an array of III-V/Si external cavity lasers is connected to a switch and a booster amplifier.

As this laser will be used to transmit and receive advanced modulation formats, the instantaneous linewidth of the laser needs to be small. This requires the use of low-loss external cavity arrangements. State-of-the-art III-V-on-silicon lasers have recently been realized with kHz-level linewidths, due to the very low waveguide losses that can be obtained on this platform [9]. In this case, the III-V semiconductor material was integrated on the silicon waveguide circuit using die-to-wafer bonding. It is difficult however to scale this technology to integrate different III-V dies on a single waveguide circuit to achieve the ultra-wide bandwidth. The Photonics Research Group of UGent is developing a new technology – micro-transfer printing – to integrate III-V semiconductor material on silicon waveguide circuits [9]. The concept of the technology is illustrated in Figure 2. This technique allows to massively parallel integrate sub-mm size III-V material/devices from its native growth substrate to a 200 mm or 300 mm silicon photonic wafer. This technique will be used in this project to co-integrate different III-V gain materials on a single silicon photonic integrated circuit. This silicon circuit will then define the different laser cavities (tuned by means of micro-heaters) as well as the switch that will determine which laser cavity is connected to the optical fibre, as shown in Figure 1.

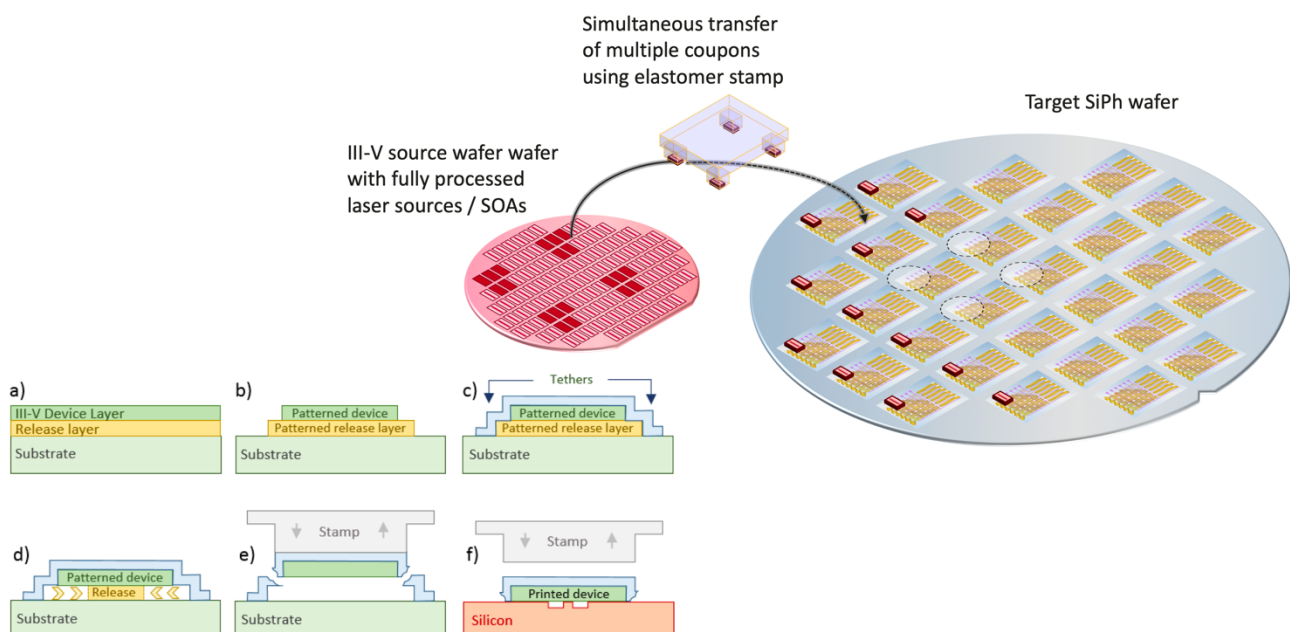


Figure 2: Concept of micro-transfer printing of III-V semiconductor devices on a silicon waveguide circuit.

## 1.2 Target Specifications of the wideband tuneable laser source

- Tuning range of the laser: > 200 nm; quasi-continuous tuning
- Output power: > 10 dBm
- Side mode suppression ratio (SMSR): > 40dB
- line width of the laser: <100 kHz
- RIN (relative intensity noise): <-130 dB/Hz

## 3. DUAL-POLARIZATION I/Q MODULATOR

### 3.1 Concept

For the WON project a dual-Polarization IQ Modulator in the Indium Phosphide (InP) material system is envisioned. The principle scheme of such a modulator can be found in Figure 3. The chip is layouted in a west/east configuration, with the RF coming from one side and the optical coupling from the other

side. North and South side of the chip can be used for DC fan out of all necessary contacts. Polarisation rotation will be done off-chip, therefore two optical outputs are present for the TE and the TM-to-be output.

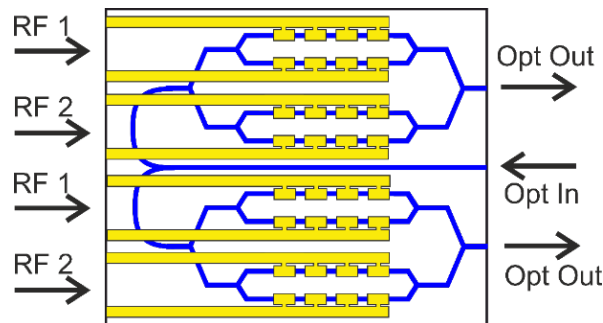


Figure 3: Principle Scheme of an InP Dual-Polarization IQ Modulator.

The breakdown of the functional elements for a single Mach-Zehnder Modulator (MZM) is depicted in Figure 4. This MZM can be nested in a second MZM forming an IQ-Modulator (IQM) using additional splitters and combiners.

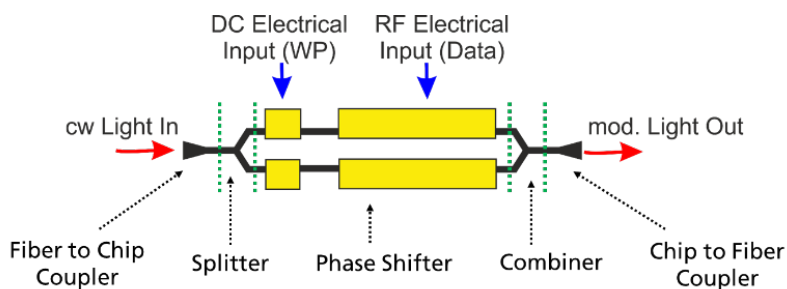


Figure 4: Breakdown of a Mach-Zehnder Modulator into its basic functional elements.

The functional elements are listed in Table 3 along with their possible implementation form. Associated parameters and their dependence on wavelength are given as well. Since the aim of the WON project is to increase the possible operating wavelength range, special attention is paid to their wavelength dependence.

Table 3: Functional Elements of a Mach-Zehnder Modulator, possible implementations and associated parameters

	Coupler from/to Chip	Splitter/Combiner	EO-Phase Shifter
<b>Implementation</b>	Taper (hor./vert.)	Y-Splitter	QCSE
		1x2 MMI	Pockels
		2x2 MMI	Plasma Effect
<b>Parameters</b>	Loss ( $\lambda$ )	Splitting Ratio ( $\lambda$ )	Phase Shift ( $\lambda$ ) = $V\pi(\lambda)$
		Loss ( $\lambda$ )	Loss ( $\lambda$ )
			RF Modulation Bandwidth

The coupling in/out from a fibre to the chip is eased by Spot-Size-Converters transferring the optical mode of the fibre to the (typically) much smaller optical mode present in the semiconductor

waveguide. Conversion can be done using horizontal and/or vertical taper structures realised on the InP chip. The loss of these tapers will be wavelength dependent but as long as for the short wavelength the mode is not pushed into the cut-off the tapers should work. Loss per coupling is estimated to be in the range of 1 - 3 dB.

The splitters can be realized either as Y-Splitter or 1×2 MMI. The Y-Splitter is smaller while the 1×2 MMI has better fabrication tolerances. Both elements offer wavelength independent splitting ratio but the loss is wavelength dependent. We favour the 1×2 MMI and estimate a maximum of 1.5dB of loss for the entire wavelength range.

The combiner is realized using a 2×2 MMI. This element is also working according to the self-imaging principle but in contrast to the 1×2 MMI not only the loss but also the splitting ratio is wavelength dependent. Here most of the design and simulation effort is necessary to improve the performance. The 2×2 MMI can either be realized as a conventional MMI in InP (see

Figure 5). From this we would estimate a maximum loss of 1.5 dB per combiner over the entire wavelength range and a splitting ratio of close to 1 for 80% of the wavelength range.

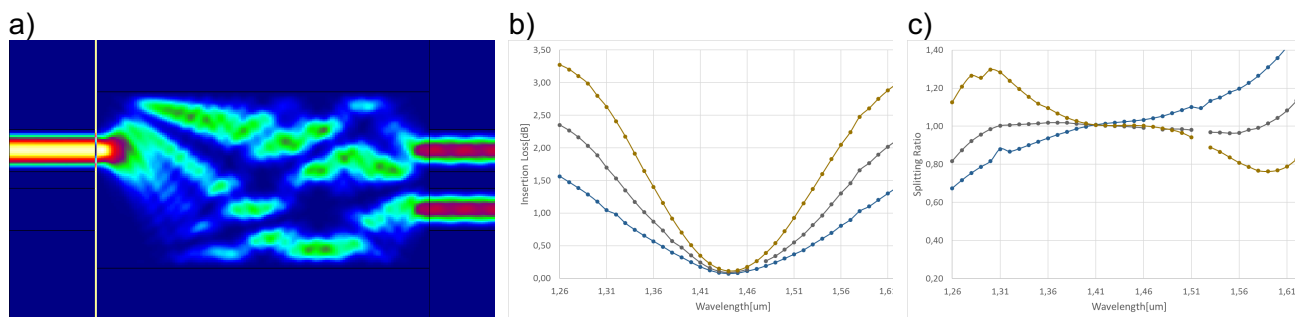


Figure 5: 2×2 MMI in InP a) color coded intensity distribution b) Loss vs wavelength c) Splitting Ratio versus wavelength.

MMIs with lower insertion loss have been published using a grating structure MMI in the Si/SiO<sub>2</sub> material system [8]. Here the loss is less than 1 dB over a range of more than 200 nm. No information on the splitting ratio is given. If and how this concept can be transferred to the InP material system will be part of the research in WON.

Within the InP material system Multi-Quantum-Wells (MQWs) are used for the eo-phase shifter. MQWs enable the Quantum-Confined Stark-Effect (QCSE), which delivers high eo phase shift values per applied voltage, resulting in low  $V_{\pi}$  values. The Pockels effect is also present but does not account for more than 25% of the overall phase shift. By carefully adjusting the MQW parameters, namely well-width, barrier width and photoluminescence wavelength an as small as possible  $V_{\pi}$  increase with increasing wavelength is targeted. In the end the insertion loss of the phase shifter and the associated  $V_{\pi}$  can be adjusted by varying the applied reverse bias to the diodes.

### 3.2 Target Specifications of the wideband dual-polarization I/Q modulator

- **Insertion Loss**  
The Insertion Loss of a single IQ Modulator is targeted not to exceed 14 dB over the entire wavelength range. That corresponds to around 15 dB from the input to the output of one polarization branch of the dual-polarization IQ Modulator.
- **Half wave Voltage ( $V_{\pi}$ )**  
 $V_{\pi}$  should not be larger than 3V

- Extinction Ratio

The extinction ratio (ER) strongly depends on the splitting ratio of the MMIs, here 15 dB ER is targeted.

ER defines the ratio between the maximum power and the power level when the output of the MZM is switched off. In an ideal IQ modulator, ER would be infinite. Given that a finite ER is associated with a power imbalance between the optical IQ modulator arms, and therefore, an imperfect SR, this work focuses its analysis on the SR parameter instead of ER. The IL quantifies the amount of light that is lost as the beam propagates through the waveguides and couplers.  $V_\pi$  is the half wave voltage and is the voltage applied to the two MZM arms, which are in push-pull configuration, to induce a phase difference of  $180^\circ$  in the two arms. Given that the studies carried out so far in this project only permit us to state that SR and IL severely vary with respect to the wavelength, the upcoming results will consider a constant  $V_\pi$ .

Since couplers are major building blocks in the design of optical IQ modulators and once it has been shown that their performance varies according to the wavelength in play, it is expected that IQ modulators can be significantly affected when wideband scenarios are considered. Previous simulations have shown (section 2.3), that insertion loss of  $1 \times 2$  MMIs can range up to almost 2 dB whereas with  $2 \times 2$  MMIs, this variation ranges up to nearly 1.7 dB (

Figure 5).

Simulations have shown that for  $1 \times 2$  MMI the splitting ratio does not depend on the wavelength as for the  $2 \times 2$  MMI, where the impact can range between 40% and 140% of the ideal value ( $SR = 1$ ). In coherent systems, the splitting ratio is a critical parameter, which introduces distortions and contributes to the overall OSNR (Optical Signal-to-Noise Ratio) penalty of a transmission system. In order to properly analyse the viability of transmission when MMI couplers are incorporated to dual-Pol IQ Modulators, simulations were conducted to investigate how the performance behaves for different optical bands.

The following simulations were carried out considering a simple coherent scheme that attempts to isolate the distortions caused uniquely by the coupler imperfections (IL and SR). As figure of merit, the required OSNR to achieve a fixed BER of  $2 \cdot 10^{-2}$  was used. A symbol rate of 32 GBaud was assumed and three different modulation format orders (4, 16 and 64) for a QAM signal were chosen. As the laser power and linewidth, until the current stage of this work, have not been specified as functions of the wavelength, it was assigned fixed values of 1 mW and 0 Hz, respectively.  $V_\pi$  was also set to a constant value and equal to 1 V.

Figure 6 shows the evaluation of the OSNR penalty (at BER of  $2 \cdot 10^{-2}$ ) as function of the wavelength for the dual-polarization (DP) IQ Modulator based on the IQ-MZM design presented in Figure 3. As can be seen, the performance is significantly influenced by the  $2 \times 2$  MMI splitting ratio behaviour ( $SR_{2 \times 2}$ ), also plotted in Figure 6 (for instructive purposes).  $SR_{2 \times 2}$  reaches its minimum at the leftmost part of the O-band ( $1.26 \mu\text{m}$ ) and its maximum at the centre of the E-band ( $1.41 \mu\text{m}$ ), respectively. As a consequence, the OSNR penalty curve increases at the beginning of the O-band. If an upper limit of 0.5 dB for the OSNR penalty is set, only 66% of the O-band would tolerate transmission of PDM-4QAM signals (at BER of  $2 \cdot 10^{-2}$ ). Moreover, the impact on the symbols is explicit, where the IQ imbalances stretch the signal towards the quadrature component direction (Figure 7). Therefore, target specifications for this system would demand the design of  $2 \times 2$  MMIs with SR limited at the minimum of 0.6, once that when going lower than this value the 0.5 dB toleration limit is extrapolated.

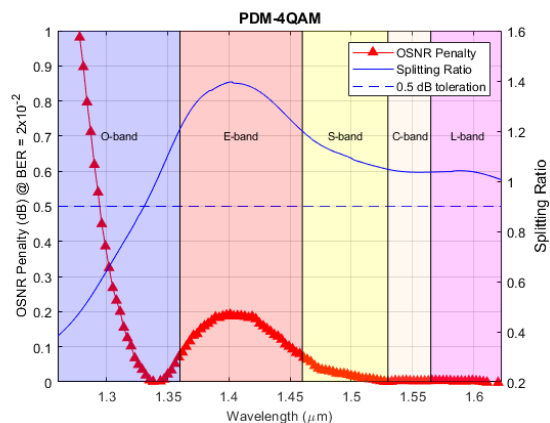


Figure 6: OSNR penalty for PDM-4QAM signal. 66% of O-band is available for transmission. SR must be above 0.6 to permit transmission with OSNR penalty lower than 0.5 dB.

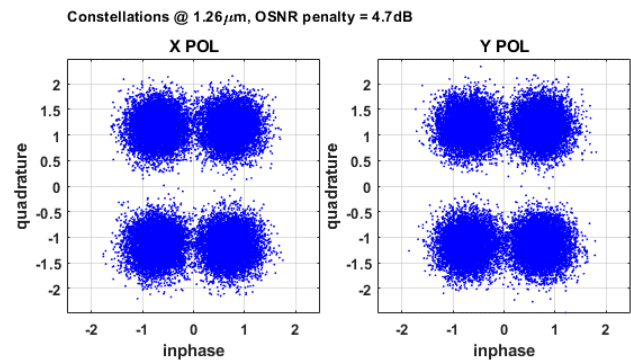


Figure 7: PDM-4QAM constellation at 1.26 μm. Signal imbalanced towards quadrature component. A 4.7 dB OSNR penalty was set for visual purposes.

By carrying out the same analysis for a PDM-16QAM signal, it is possible to see that OSNR penalties in the E and S-band increase. Now, only 32% of O-band is available for transmission as well as 83% of S-band. The E-band is completely infeasible. For PDM-16QAM, the target specification of the SR must be between roughly 0.9 and 1.1 to permit transmission with an OSNR penalty lower than 0.5 dB.

Finally, a more complex modulation format (PDM-64QAM) was simulated (Figure 9). 14% of O-band, 0% of E-band and 23% of S-band are available for transmission. The target specification of the SR must be between 0.94 and 1.06, which shows a very limited tolerance interval compared to PDM-4QAM.

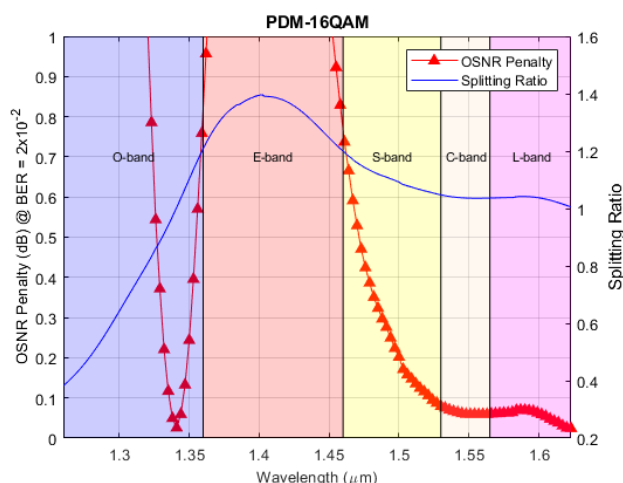


Figure 8: OSNR penalty for PDM-16QAM signal. 32% of O-band, 0% of E-band and 83% of S-band are available for transmission. SR must be above 0.9 and lower than 1.1 to permit transmission with OSNR penalty lower than 0.5 dB.

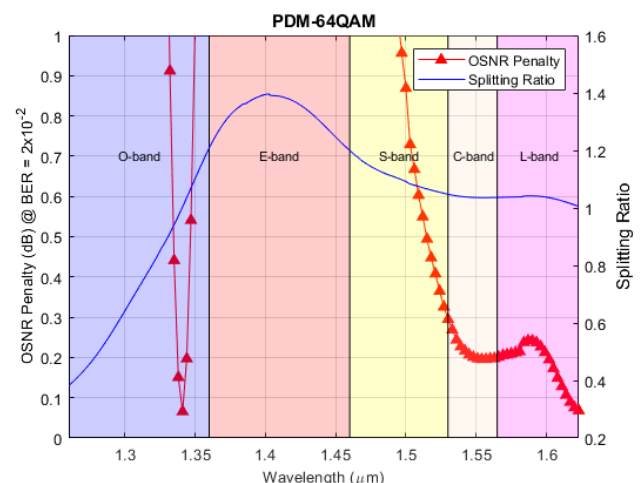


Figure 9: OSNR penalty for a PDM-64QAM signal. 14% of O-band, 0% of E-band and 23% of S-band are available for transmission. SR must be above 0.94 and lower than 1.06 to permit transmission with OSNR penalty lower than 0.5 dB.

To summarize the results discussed so far, Table 4 shows the spectrum availability per band for the assumed scenario and Table 5 the respective tolerated splitting ratio values.

Table 4: Spectrum availability per band at 0.5 dB of OSNR penalty.

Band	PDM-4QAM	PDM-16QAM	PDM-64QAM
O-band	66%	32%	14%
E-band	100%	0%	0%
S-band	100%	83%	23%
C-band	100%	100%	100%
L-band	100%	100%	100%

Table 5: 2×2 MMI permitted splitting ratio range.

	PDM-4QAM	PDM-16QAM	PDM-64QAM
SR range	> 0.6	[0.90, 1.10]	[0.94, 1.06]

#### 4. INTRADYNE COHERENT RECEIVER FRONTEND

In the design of wideband transceivers, the importance of RXs cannot be neglected. Besides that, it is well-known that L-band receivers are already a reality [10], but the effort to further expand beyond C+L has become a target of study in recent researches [7].

The challenge in determining target specifications for wideband transceivers is associated with the material properties. Currently, group III-V modulators, such as InP, have been largely employed in transceiver design due to its already mentioned properties (e.g., low driving voltage and small footprint). However, the limitation in terms of bandwidth (up to 40 nm) restricts the expansion to other bands rather than C. On the other hand, group IV components, such as silicon photonic, permit ten times more bandwidth (400 nm). Furthermore, these group IV modulators also use carrier depletion for modulation, then when used with wideband couplers [12], it is possible to mitigate the effects discussed in section 0 and grant signal integrity from O to L band. Back to the receiving side, a limiting factor in the use of silicon photonic photodetectors is that in the ones that harness unstrained Ge, the absorption curve starts to roll-off at nearly 1570 nm. However, studies [13] have shown that the use of strained Ge shifts the roll-off point to longer wavelengths and permit the operation over a wide optical bandwidth.

The device developed in [7], which is based on SiPh PIC (Photonic Integrated Circuit), provides a good forecast of target specifications for wideband receivers. The device permits received power level in the range of -25 dBm up to -21dBm for a 16QAM (at BER of  $1 \cdot 10^{-3}$ ). The receiver considered within the study is able to operate over 370 nm with 3.5 dB variation in receiver loss over all polarizations. In regards to LO (local oscillator) specifications, a good forecast can be found in section 2.2. Therefore, the design proposed shows promising roadmaps towards the route of silicon photonics, nonetheless, when the state-of-the-art for multi-band systems nowadays (mostly L-band) is analysed, In-P based technologies still pose as main protagonists.

In the design of optical 90 degree hybrid for L-band, a good forecast of current target specifications can be found in [10], [14]. For phase-error, for instance, acceptable values range are  $\pm 7.5$  degrees. As for the receiver responsivity, the tolerable range is between 0.05 and 0.1 A/W. Finally, in terms of polarization extinction ratio, the minimum permitted is 20 dB.

## 5. DIGITAL SIGNAL PROCESSING

### 5.1 Transmitter-Side DSP

Digital signal processing at the transmitter plays a fundamental role in any modern transponder. Besides the already mentioned filtering and encoding, within the DSP there are other important blocks that improve the overall quality of transmission. There are two parts that need to be differentiated and discussed separately: (I) the digital communication techniques that are used for transmission and (II) the DSP that it is utilized to compensate for the components and fiber propagation effects.

The main difference when moving from C- (single band, narrow spectrum) to multi-band O to L-band systems is that the fiber and component characteristics are not uniform anymore. In reality, this happens always, but being the C-band only 35 nm wide, the frequency dependent variations are not too large and therefore compensable by the DSP at the receiver. In the previous sections, for example, the frequency dependent behaviour of the MZM has been described, similarly, fundamental parameters of the optical fiber, e.g., dispersion and attenuation vary over frequency. For instance, the C-band presents the minimum loss of the entire spectrum, while the dispersion is high enough to limit the impact of nonlinear Kerr effect in current commercial systems. On the other hand, when we transmit for example within the O-band, the attenuation is, in dB, almost twice as high as in C-band, and the dispersion reaches the zero point within the O-band. In this spectral area, current system could not be efficiently utilized.

In this context utilization of different digital communication and DSP must be considered. For what concerns digital communication, it will be necessary to enable the transponder to transmit different modulation formats, so that for each spectral area we can consider the optimal one. This can be achieved by techniques such as digital subcarrier multiplexing, time-hybrid formats, multi-dimensional formats, and probabilistic shaping. All of them, to be properly used, must be supported by a proper software defined controller that can automatically set the parameters given the current channel conditions.

On the DSP side, digital pre-emphasis, digital pre-distortion and advanced pilot tone techniques could be considered to limit the penalties introduced in a multi-band system by fiber propagation and components. Digital pre-emphasis enable the compensation of bandwidth limitation and it could be beneficial to guarantee that all channels generated with similar spectral characteristics. For what concern digital pre-distortion, we will consider analytical methods based on the gradient approach or Volterra filters. Neural networks will be considered as well. Similarly, we will consider neural network to pre-distort the channel, and thus optimizing it, with respect to the channel before it is propagated. The latter methods will be particularly relevant when the channel will be allocated within the O-band, where the dispersion is around zero, and therefore nonlinear effects play a fundamental role in the overall channel nonlinear effects.

### 5.2 Receiver-Side DSP

At the receiver side, the structure of the DSP will not change considerably with respect to current ones. The chain of components as described in Fig. 2 will remain unchanged also in a multi-band system, with some minor variations.

In a coherent DSP-based receiver an important role is played by frequency domain equalizer. Being the amount of dispersion considerably different in multi-band after transmission, this block might need to be re-designed. On the other hand, the impact of nonlinear effects will be different over the entire

spectrum. In fact, because of the broadband nonlinear effect which goes under the name of stimulated Raman scattering, the low wavelength channels will transfer power to the higher wavelengths. This means that the channels in O-band will essentially work in linear regime, while the ones in L-band in nonlinear one. To address these differences, proper nonlinear equalizers, also based on neural networks, will be studied within WON.

## REFERENCES

- [1] “Cisco visual networking index: Forecast and methodology, 2015–2020,” White Paper, 2015.
- [2] Inniss, Daryl & Rubenstein, Roy. (2017). Data Center Architectures and Opportunities for Silicon Photonics. 10.1016/B978-0-12-802975-6.00007-7.
- [3] Yutaka Miyamoto, Shuichi Yoshino, and Akira Okad (2019) 'Ultrahigh-speed Transmission Technology for Future High-capacity Transport Networks', NTT Technical Review, 17(5), pp. [Online]. Available at: <https://www.ntt-review.jp/archive/ntttechnical.php?contents=ntr201905fa1.html> .
- [4] Han Sun et al., “800G DSP ASIC Design Using Probabilistic Shaping and Digital Sub-Carrier Multiplexing”, IEEE / OSA J. of Lightwave Technology
- [5] Hamaoka, Fukutaro & Nakamura, Masanori & Okamoto, Seiji & Minoguchi, Kyo & Sasai, Takeo & Matsushita, Asuka & Yamazaki, Etsushi & Kisaka, Yoshiaki. (2019). Ultra-Wideband WDM Transmission in S, C, and L-bands Using Signal Power Optimization Scheme. Journal of Lightwave Technology. PP. 1-1. 10.1109/JLT.2019.2894827.
- [6] Ferrari, Alessio, et al. "Assessment on the Achievable Throughput of Multi-band ITU-T G. 652. D Fiber Transmission Systems." Journal of Lightwave Technology (2020).
- [7] C. Doerr, L. Chen, T. Nielsen, R. Aroca, L. Chen, M. Banaee, S. Azemati, G. McBrien, S. Y. Park, J. Geyer, B. Guan, B. Mikkelsen, C. Rasmussen, M. Givehchi, Z. Wang, B. Potsaid, H. C. Lee, E. Swanson, and J. G. Fujimoto, "O, E, S, C, and L Band Silicon Photonics Coherent Modulator/Receiver," in *Optical Fibre Communication Conference Postdeadline Papers*, OSA Technical Digest (online) (Optical Society of America, 2016), paper Th5C.4.
- [8] Halir, Robert & Cheben, Pavel & Luque-González, José & Sarmiento-Merenguel, Jose & Schmid, Jens & Wangüemert-Pérez, Gonzalo & Xu, DanXia & Wang, ShuRui & Ortega-Moñux, Alejandro & Molina-Fernández, Iñigo. (2016). Ultra-broadband nanophotonic beamsplitter using an anisotropic sub-wavelength metamaterial. Laser & Photonics Reviews. 10. 1039-1046. 10.1002/lpor.201600213.
- [9] M. Tran, D. Huang, J. Bowers, Tutorial on narrow linewidth tunable semiconductor lasers using Si/III-V heterogeneous integration, APL Photonics 4, 111101 (2019)
- [10] J. Zhang, G. Muliuk, J. Juvert, S. Kumari, J. Goyvaerts, B. Haq, C. Op de Beeck, B. Kuyken, G. Morthier, D. Van Thourhout, R. Baets, G. Lepage, P. Verheyen, J. Van Campenhout, A. Gocalinska, J. O'Callaghan, E. Pelucchie K. Thomas, B. Corbett, A. Jose Trindade, G. Roelkens, III-V-on-Si photonic integrated circuits realized using micro-transfer-printing, APL Photonics 4, 110803 (2019)
- [11] Gotoh, M. & Sakurai, K. & Kurokawa, M. & Ashizawa, K. & Yoneda, Y. & Fujimura, Y.. (2018). Coherent receiver for L-band. SEI Technical Review. 48-53.
- [12] J. K. S. Poon, W. D. Sacher, Y. Huang, and G.-q. Lo, “Integrated Photonic Devices and Circuits in Multilayer Silicon Nitride-on-Silicon Platforms,” vol. 1, no. c, pp. 3–5, 2015.
- [13] J. Liu, J. Michel, W. Giziewicz, D. Pan, K. Wada, D. D. Cannon, S. Jongthammanurak, D. T. Danielson, L. C. Kimerling, J. Chen, F. O' . Ilday, F. X. Ka'rtner, and J. Yasaitis, “High-performance, tensile-strained Ge p-i-n photodetectors on a Si platform,” Applied Physics Letters, vol. 87, no. 10, 2005.
- [14] T. Okimoto et al., “InP-based Waveguide Photodetector Monolithically Integrated with 90° Hybrid Having High-responsivity Characteristics over the L-band Wavelength Range,” The 2017 IEICE Electronics Society (C-4-11).